Clinical Chemistry 61:2
420–429 (2015)

Digital Microfluidic Platform for the Detection of Rubella Infection and Immunity: A Proof of Concept

Alphonsus H.C. Ng,[1,3] Misan Lee,[2,3] Kihwan Choi,[3,4] Andrew T. Fischer,[5] John M. Robinson,[6] and Aaron R. Wheeler[1,3,4*]

BACKGROUND: Whereas disease surveillance for infectious diseases such as rubella is important, it is critical to identify pregnant women at risk of passing rubella to their offspring, which can be fatal and can result in congenital rubella syndrome (CRS). The traditional centralized model for diagnosing rubella is cost-prohibitive in resource-limited settings, representing a major obstacle to the prevention of CRS. As a step toward decentralized diagnostic systems, we developed a proof-of-concept digital microfluidic (DMF) diagnostic platform that possesses the flexibility and performance of automated immunoassay platforms used in central facilities, but with a form factor the size of a shoebox.

METHODS: DMF immunoassays were developed with integrated sample preparation for the detection of rubella virus (RV) IgG and IgM. The performance (sensitivity and specificity) of the assays was evaluated with serum and plasma samples from a commercial antirubella mixed-titer performance panel.

RESULTS: The new platform performed the essential processing steps, including sample aliquoting for 4 parallel assays, sample dilution, and IgG blocking. Testing of performance panel samples yielded diagnostic sensitivity and specificity of 100% and 100% for both RV IgG and RV IgM. With 1.8 μL sample per assay, 4 parallel assays were performed in approximately 30 min with $<$10% mean CV.

CONCLUSIONS: This proof of concept establishes DMF-powered immunoassays as being potentially useful for the diagnosis of infectious disease.

Vaccine-preventable infectious diseases such as measles, mumps, and rubella continue to be a global threat because many developing countries have low or nonexistent immunization coverage *(1)*. Although rubella is manageable for most adults and minors (rash, fever, and flu-like symptoms), rubella infection during pregnancy has significant risk of causing fetal death and/or a debilitating suite of defects known as congenital rubella syndrome (CRS)[7] *(2)*; $>$100 000 infants are born with CRS each year *(3)*.

As is the case for many infectious diseases, screening for rubella susceptibility, immunity, and infection is challenging, requiring the selective detection of rubella virus (RV)-specific IgG and IgM. Because the test components of RV IgM immunoassays can cross-react with other biogenic proteins [e.g., RV IgG or rheumatoid factor (RF) IgM], there is a high occurrence of false-negative or false-positive results, depending on the quality of the assays and the experience of the operators *(4–6)*. Thus, although there are portable tests available *(7)*, rubella is almost always diagnosed in central clinical laboratories. In resource-limited settings, transportation from rural communities to remote laboratories is often cost prohibitive *(8)*, meaning that rubella infections (and attendant cases of CRS) routinely sweep through rural populations without testing or treatment *(9)*.

Given the challenges described above, there is great enthusiasm for moving to decentralized systems for disease diagnosis and surveillance. This model requires portable assays, and the microfluidic (or "lab on a chip") community has attempted to address this challenge primarily through systems that rely on fluid flow through enclosed microchannels *(10–12)* or lateral flow through a paper-based absorptive matrix *(13–15)*. Microchannel-based systems have excellent analytical sensitivity *(16)* and proven diagnostic performance in

[1] Institute of Biomaterials and Biomedical Engineering, [2] Innis College, and [4] Department of Chemistry, University of Toronto, Toronto, ON, Canada; [3] Donnelly Centre for Cellular and Biomolecular Research, Toronto, ON, Canada; [5] Abbott Diagnostics, Irving, TX; [6] Abbott Diagnostics, Abbott Park, IL.
* Address correspondence to this author at: University of Toronto, 80 St. George St. Toronto, ON, Canada M5S 3H6. Fax 416-946-3865; e-mail aaron.wheeler@utoronto.ca.
Received August 27, 2014; accepted November 13, 2014.
Previously published online at DOI: 10.1373/clinchem.2014.232181

[7] Nonstandard abbreviations: CRS, congenital rubella syndrome; RV, rubella virus; RF, rheumatoid factor; DMF, digital microfluidics; Cal, calibrator; HRP, horseradish peroxidase; PMT, photomultiplier tube; LOD, limit of detection; LOQ, limit of quantification; s/co, signal-to-cutoff ratio; EIA, enzyme immunoassay; RLU, relative light unit.

resource-limited settings *(17–19)*, but often require extensive ancillary equipment to operate (e.g., pumps, flow meters, and valves) and intricate device fabrication for integrated sample preparation *(20)*. In contrast, paper-based systems can be simple and inexpensive to manufacture and use *(21)*, but adequate analytical performance in such devices has been demonstrated for only a few analytes *(15)*, and multistep liquid manipulation with uniform flow profiles requires careful material manipulation and device design *(22–24)*.

An alternative to (channel-based or lateral) fluid flow for miniaturized analysis systems is a technology known as digital microfluidics (DMF) *(25–27)*, in which sample and reagents are manipulated as discrete droplets on a hydrophobic surface. DMF systems actuate droplets through the application of electrical potentials on a generic array of insulated electrodes—a format that enables software-reconfigurable, concurrent droplet operations including merging, mixing, splitting, and metering from reservoirs *(28)*. DMF devices can be cost-effectively fabricated on paper by inkjet printing *(29)* and can be operated with simple and compact instrumentation *(30, 31)* with no need for pumps, interconnects, valves, or fittings. Although these advantages have motivated the development of DMF-powered immunoassays for small-molecule and protein biomarkers *(32–35)*, we are not aware of DMF immunoassays being used for diagnosis of infectious diseases.

Here, we report the development of DMF-powered RV IgG and RV IgM immunoassays, with a focus on evaluating the diagnostic performance of DMF immunoassays relative to central laboratory methods. These assays use RV-immobilized magnetic particles to capture the analyte from the sample and enzyme-linked detection antibodies to transduce analyte-binding events to chemiluminescent signal. All assay steps, from sample to analysis, were performed by DMF with a shoebox-sized prototype instrument. We propose that this represents a useful step toward the development of decentralized diagnostic tools for the diagnosis of rubella and other infectious diseases.

Materials and Methods

REAGENTS AND MATERIALS

Unless otherwise specified, we purchased reagents from Sigma-Aldrich. Deionized water had a resistivity of 18 MΩ · cm at 25 °C. Pluronic L64 (BASF Corp.) was generously donated by Brenntag Canada.

We adapted most immunoassay reagents from the Architect rubella IgM and IgG assay kits from Abbott Laboratories, including RV IgG calibrators, RV IgM cutoff Calibrator 1 (Cal 1), RV IgM pretreatment reagent containing goat antihuman IgG, and virus-coated paramagnetic microparticles. Reagents from other vendors included Superblock Tris-buffered saline and SuperSignal ELISA Femto chemiluminescent substrate, comprising stable peroxide (H_2O_2) and luminol-enhancer solution, from Thermo Fischer Scientific; antirubella mixed-titer performance panel (PTR201-00-0.5) from SeraCare Life Sciences; and defibrinated sheep blood from Quad Five.

We prepared custom digital microfluidic compatible wash buffer and conjugate diluent as described previously *(32, 33)*. Conjugate working solutions for RV IgG or RV IgM assays were formed by diluting horseradish peroxidase (HRP)-conjugated goat polyclonal antihuman IgG (21 ng/mL) or HRP-conjugated goat antihuman IgM (23 ng/mL), respectively, in conjugate diluent. Pretreatment working solution was formed from a 3× dilution of IgM pretreatment reagent in conjugate diluent. The microparticle working suspension was formed in an Eppendorf tube by removing the original diluent (with particles immobilized with a neodymium magnet), washing the particles twice in Superblock, and resuspending the washed particles in Superblock at 1.5×10^8 particles/mL (approximately 10× the stock concentration). Simulated whole blood samples were formed from a 1:1 mixture of RV IgG calibrator and sheep blood. Before running immunoassays, we diluted calibrators, simulated whole-blood samples, or patient samples (from performance panel) 10× in Dulbecco PBS containing 4% BSA. All reagents used on digital microfluidic devices or on-chip were supplemented with Pluronic L64 at 0.05%.

DEVICE FABRICATION AND OPERATION

We used a custom automation system with approximate dimensions 7 × 9 × 12 inches to manage droplet operation, magnet and photomultiplier tube (PMT) position, and data collection (Fig. 1A) *(30, 32)*. Digital microfluidic devices, comprising a top plate and bottom plate, were fabricated in the University of Toronto Nanofabrication Centre cleanroom facility and assembled as described previously *(32)* (Fig. 1B). The bottom plate device design featured an array of 80 actuation electrodes (2.54 × 2.54 mm) connected to reservoir electrodes for sample and reagent storage and waste removal. Unit droplet volumes on the actuation electrodes were approximately 900 nL, as determined by the area of each actuation electrode and the gap spacing (approximately 140 μm) between the top plate and bottom plate.

Droplets were actuated by applying a preprogrammed sequence of driving voltages (80–100 V_{RMS} 10 kHz sine wave) between the top plate (ground) and electrodes in the bottom plate through a Pogo pin interface (90 pins). For on-chip particle separation, a motorized magnet system called a magnetic lens *(32)* is positioned approximately 150 μm underneath the device. In this activated state, >600 μN of magnetic force is sufficient to focus particles into a pellet, immobilizing them on the

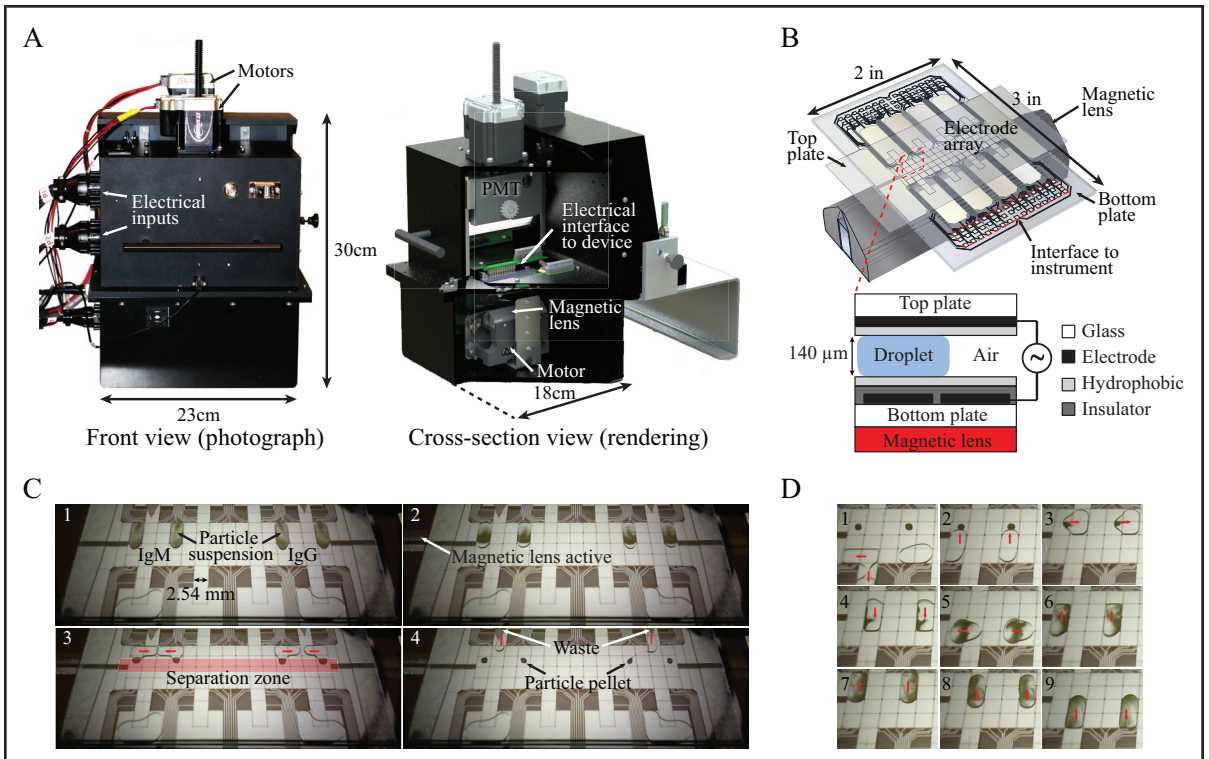

Fig. 1. Automated digital microfluidic platform.

(A), Left: Photo of automation system (front view) showing the position of electrical inputs from the DropBot *(30)* and external motors that control the PMT and enclosure. Right: Cross-section computer-aided design rendering showing the interior components of the system, including the PMT, the magnetic lens, and the motor system that controls the position of the magnetic lens. (B), Three-dimensional schematic and side view of digital microfluidic device positioned above the magnetic lens. (C), Video sequence of digital microfluidic magnetic separation of paramagnetic particles in parallel RV IgM and RV IgG immunoassays (see online Supplemental Video 1). (D), Video sequence of resuspending and mixing of particles in wash buffer solution. Red arrows indicate the direction of droplet movement.

surface (Fig. 1C; also see Supplemental Video 1, which accompanies the online version of this article at http://www.clinchem.org/content/vol61/issue2). With digital microfluidic actuation, the supernatant can be separated from the particles, provided that the immobilization force exceeds the minimal threshold (approximately 500 μN) required to overcome the surface tension of the droplet *(32, 33)*. The particle pellet is resuspended by deactivating the magnetic lens (i.e., magnet is positioned 3.8 cm below the device) and moving and mixing a droplet over the particles (Fig. 1D).

To measure on-chip chemiluminescence, the reaction droplet is moved to the center of the electrode array and a motorized PMT is positioned several hundred micrometers above the device to collect light from the droplet. When the PMT is inactive (i.e., the PMT is positioned 5 cm above the device), an integrated light-emitting diode and webcam assembly is used to monitor on-chip droplet movement. We implemented 3 design measures to prevent users from damaging the PMT, including (*a*) 2 sensors to ascertain the position of the PMT, (*b*) a shutter mechanism to prevent light from saturating the sensor when it is not in use, and (*c*) deep grooves in the enclosure to ensure that the instrument is light-tight during measurements.

RV IgG IMMUNOASSAY

RV IgG antibodies were detected on-chip with an indirect ELISA comprising 7 steps. (*a*) A droplet of virus-coated paramagnetic particle suspension (1.8 μL) was dispensed from a reservoir, and the particles were separated from the diluent. (*b*) A droplet of sample (1.8 μL, containing RV IgG) was dispensed, delivered to the particles, mixed for 3 min, and separated from particles. (*c*) The particles were washed in 4 successive droplets of wash buffer (i.e., 4 × 1.8 μL), each time mixing and then separating from the supernatant. (*d*) A droplet of HRP conjugate solution (1.8 μL, containing HRP-conjugated antihuman IgG) was dispensed, delivered to the particles, and mixed for 2 min. (*e*) Step c was repeated. (*f*) One

droplet each of H_2O_2 (900 nL) and luminol-enhancer solution (900 nL) were dispensed and merged with the particles; the solutions and particles were mixed for 2 min. (*g*) The mean chemiluminescent signal over 10 s was obtained with the integrated PMT.

By aliquoting 4 sets of samples and reagents (see online Supplemental Fig. 1), 4 parallel tests were run simultaneously (i.e., steps a–g were performed in parallel for 4 samples). Applying this protocol, a calibration curve for RV IgG was established in 4 replicates (intraassay), with calibrator solutions containing 0, 5, 10, 15, 75, and 250 IU/mL RV IgG. The limits of detection (LOD) and quantification (LOQ) for this assay were the concentrations corresponding to the position on the calibration curve of the mean signal generated from blank measurements plus 3 (LOD) or 10 (LOQ) times the SD of the blank measurements. A set of calibration data was used for repeated experiments until a new batch of devices or magnetic particles were introduced, or when the control sample measurements were observed to be out of range. In practice, this allowed the use of each set of calibration data for >200 experiments over 50 days.

INTEGRATED ON-CHIP DILUTION AND RV IgG IMMUNOASSAY

As shown in online Supplemental Fig. 2, samples were diluted on-chip in 3 iterating steps. (*1*) A droplet of sample (1.8 μL) and a droplet of diluent (1.8 μL, Dulbecco PBS 4% BSA) were dispensed, merged, and mixed. (*2*) The pooled sample droplet (2× diluted) was split into 2 subdroplets. (*3*) One sample subdroplet was stored for later analysis, and the second sample subdroplet was used to repeat steps 1–3 until the desired dilutions were achieved. For example, 4 repetitions generate 4 droplets with 2×, 4×, 8×, and 16× dilution of original sample. After dilution, RV IgG immunoassays were performed, with the 7-step (a–g) procedure above, by delivering the diluted samples to virus-coated particles. When the particles were washed, the regions on the device used for dilution and sample storage were also washed with additional wash buffer to prevent cross-contamination.

A fully integrated protocol, including dilution in 4 iterations of steps 1–3 followed by RV IgG immunoassays in steps a–g, was evaluated with a RV IgG calibrator and a simulated whole-blood sample (1:1 mixture of RV IgG calibrator and sheep blood), both containing 250 IU/mL of RV IgG. Here, on-chip dilution was performed to generate droplets containing 15.6, 31.3, 62.5, and 125 IU/mL RV IgG. For each sample (calibrator and whole blood), the protocol was repeated on 3 different devices (i.e., 3 interassay replicates).

OFF-CHIP RF IgM SCREENING

We used an RF IgM ELISA (Orgentec Diagnostika) according to manufacturer's instructions to screen for RF IgM in the RV IgG calibrators and RV IgM Cal 1. In these experiments, at least 2 replicates were evaluated for each sample by absorbance, measured at 450 nm (reference 650 nm) with a Sunrise microplate reader (Tecan) in "Accuracy" read mode. We estimated the RF IgM concentrations of the samples from a calibration curve, generated by fitting the absorbance of the ELISA calibrator solutions to a 4-parameter logistic equation.

RV IgM IMMUNOASSAY

The DMF RV IgM immunoassay was identical to the 7-step protocol (a–g) described above, except that the conjugate solution contained HRP-conjugated antihuman IgM (instead of IgG) and the sample was pretreated with antihuman IgG (before step a). In the pretreatment procedure, a droplet of sample (1.8 μL) and a droplet of pretreatment reagent (0.9 μL) were merged and mixed for 7 min. The assay was evaluated with and without pretreatment with 4 test samples: (*i*) 0 IU/mL RV IgG calibrator (control), (*ii*) 250 IU/mL RV IgG calibrator (IgG), (*iii*) 1:1 mixture of Cal 1 and 0 IU/mL RV IgG calibrator (IgM), and (*iv*) 1:1 mixture of Cal 1 and 500 IU/mL RV IgG calibrator (IgM + IgG). For each sample, 4 intraassay replicates were performed for each condition tested. The results (for IgG, IgM, and IgG + IgM) were reported as fold change, which was obtained by normalizing the signal intensity of each assay to the average signal intensity of the respective control experiments.

Applying the integrated RV IgM protocol (including both pretreatment and immunoassay), we established the cutoff calibration data in 3 replicates with unmodified Cal 1. In addition, the background signal of the RV IgM assays was evaluated in 4 replicates (intraassay) with a 0 IU/mL RV IgG calibrator.

ANTIRUBELLA MIXED-TITER PERFORMANCE PANEL

We estimated the diagnostic accuracy of DMF RV IgG and RV IgM immunoassays with 25 plasma/serum samples (PTR201-01-25, SeraCare Life Sciences). Serum or plasma samples were thawed and aliquoted into single-use vials for DMF immunoassays. Working solutions including microparticles, conjugates, and chemiluminescent substrates were made fresh each day from stock solutions.

DMF immunoassay analyses for the panel samples were completed by 3 different operators over a 1-month period. Each assay was carried out in 3–4 replicates in parallel, and operators were blinded to the reference result until all of the data were collected. The DMF assay results were reported as signal-to-cutoff ratio (s/co) values, calculated by normalizing the mean signal intensity of each assay to the mean signal intensity of the respective cutoff control. The cutoff controls for RV IgG and RV IgM assays were the 10 IU/mL RV IgG calibrator and the RV IgM cutoff Cal 1 (both included in the respective

kits), respectively. A DMF s/co ≥1 was interpreted as positive, a DMF s/co in the gray zone (0.69–0.99 for IgG and 0.75–0.99 for IgM) was interpreted as equivocal/indeterminate, and a DMF s/co below the gray zone (<0.69 for IgG and <0.75 for IgM) was interpreted as negative.

EVALUATION OF DIAGNOSTIC ACCURACY

We calculated the diagnostic sensitivity and specificity for the DMF immunoassays with the Abbott enzyme immunoassay (EIA) as a reference testing method *(36)*. For cases in which the calculated sensitivity or specificity was equal to 1, a *P* value of 0.999 was used to calculate 95% CIs, as recommended by WHO *(37)* and others *(17, 18)*.

Results and Discussion

DIGITAL MICROFLUIDIC INSTRUMENTATION

Motivated by the need to identify patients at risk for CRS, we developed DMF immunoassays for RV-specific immunoglobulins. The challenging nature of this application, which includes the need to distinguish between RV IgG and RV IgM, necessitates a sophisticated system capable of handling a large number of reagents and performing a complex series of processing steps. To achieve suitable levels of processing sophistication in a miniaturized instrument, we adapted an in-house designed computer-controlled instrument *(32)* powered by DropBot *(30)*, an open-source DMF automation system.

The shoebox-sized instrument comprises a motorized PMT for chemiluminescent detection, an electronic interface to the DropBot for droplet movement, and a magnet assembly (called a magnetic lens) for particle separation (Fig. 1A). Movement of protein-containing droplets through an air-filled device (Fig. 1B), which allows for more efficient particle-concentration and analyte washing than the more common methods relying on oil-filled devices *(33)*, is facilitated by the inclusion of Pluronic additives in samples and reagents, which reduces protein adsorption and limits cross-contamination *(38)*. During particle separation, particles in the droplet are immobilized on the surface in a region above the magnet, referred to as the separation zone (Fig. 1C; online Supplemental Video 1). Subsequently, the droplet is actuated away to waste, leaving behind a particle pellet. For particle resuspension, the magnetic lens is deactivated, and a new droplet is actuated over the particle pellet and mixed in a circular motion; this is sufficient to break up the particle pellet and completely reconstitute the particles in suspension (Fig. 1D).

The DMF instrumentation and devices described here are prototype designs used to demonstrate the diagnostic performance of DMF immunoassays. In ongoing work, we are developing next-generation systems that may be suitable for portable testing in the field [i.e., low cost, user friendly, battery-powered, and compact *(39)*]. These new designs will likely benefit from the development of low-cost device fabrication methods *(29)*, simple instrumentation *(30, 31)*, and integrated electrochemical sensors *(40, 41)*.

RV IgG IMMUNOASSAY AND SAMPLE DILUTION

Whether acquired naturally or induced by vaccination, the persistence of RV IgG antibody confers protection against rubella infection. The WHO interpretation of RV IgG serological results is dependent on the antibody concentration: a sample is positive if antibody concentration is >10 IU/mL, equivocal if it is between 5 and 10 IU/mL, and negative if it is <5 IU/mL. Individuals with antibody concentrations <10 IU/mL are susceptible to clinical illness on exposure to rubella virus. As such, testing women for RV IgG before conception or at their first antenatal visit can help minimize the risk of CRS.

Using the particle separation and resuspension techniques described above, we developed a 7-step DMF indirect ELISA for RV IgG, in which samples or reagents are aliquoted to the particles for 4 parallel assays (see online Supplemental Fig. 1). As shown in Fig. 2A, RV IgG antibodies present in the sample bind to the RV-coated paramagnetic particles. After incubation and washing, HRP-conjugated antihuman IgG is added to form immunocomplexes. After another incubation and wash cycle, hydrogen peroxide and luminol-enhancer solutions are added to the particles, and the resulting chemiluminescence is measured as relative light units (RLUs). This assay procedure, including determination of diluent compositions, reagent concentrations, incubation times, droplet operations, and chemiluminescent signal generation, was developed from design of experiment optimization *(32)*. The use of chemiluminescence is particularly advantageous because few optical components are required (e.g., no excitation source, filters, or lenses).

The assay described here was designed for detection of RV in patient serum and plasma samples. Thus, to optimize and calibrate the method, we used commercial calibrators designed to simulate human serum (buffer containing 4% BSA). As shown in the calibration curve (Fig. 2B), a direct relationship exists between the RLUs detected by the integrated PMT and the amount of RV IgG in the calibrators. The calibration curve had a dynamic range of approximately 2 orders of magnitude, the intraassay CVs ranged from 0.3% to 6.5%, and the LOD and LOQ of the assay were 0.03 and 0.1 IU/mL, respectively, below the clinical cutoff concentrations described above. Each set of 4 assays requires approximately 25 min to complete.

In some instances, samples with high analyte concentration must be diluted before analysis to facilitate

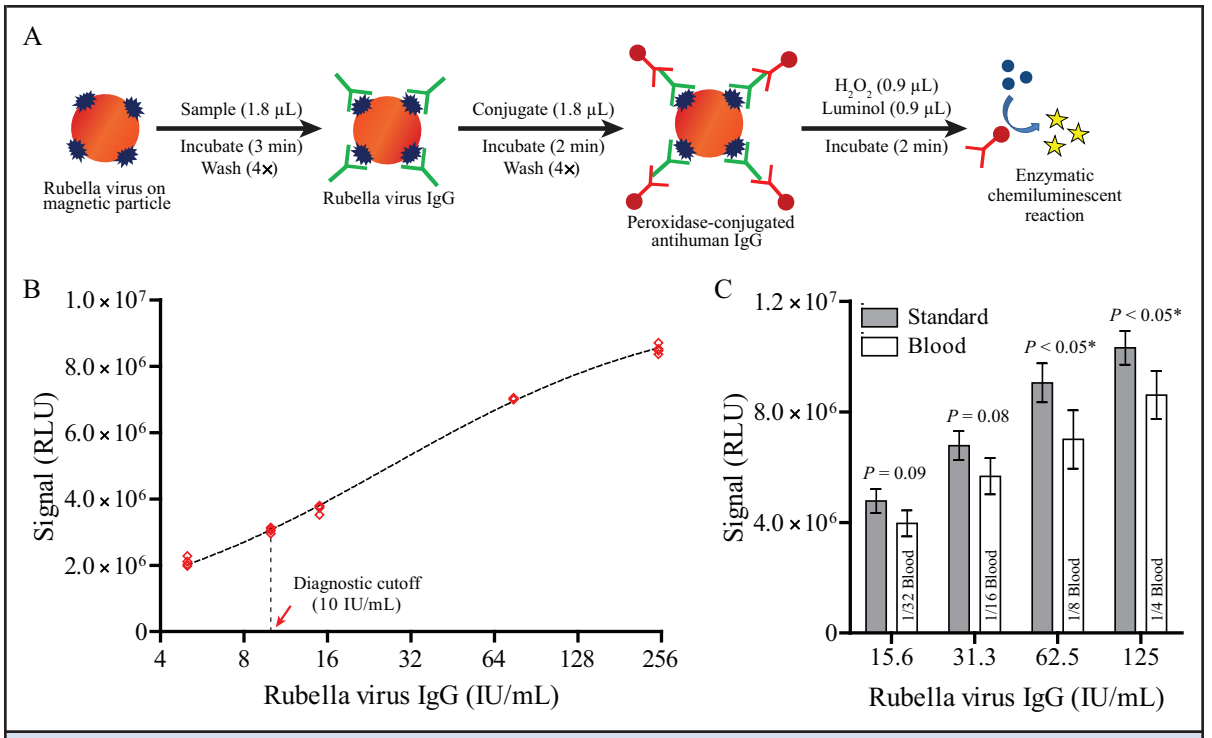

Fig. 2. RV IgG immunoassay.

(A), Scheme and procedure of RV IgG immunoassay on paramagnetic particles. (B), Calibration data (red diamonds) and curve (dotted line) for RV IgG immunoassay implemented in the digital microfluidic system. (C), Comparison of RV IgG immunoassay results for samples in calibrator solution (gray) and blood (white) for dilutions formed on-chip. Each value represents the mean (SD) from 3 replicates. Statistical significance (*$P < 0.05$) was evaluated by Student 2-tailed *t*-test.

accurate quantification; this technique is relatively trivial for central laboratories, but is not commonly used in portable tests. Hence, we evaluated whether the DMF platform could reliably perform a range of dilutions on samples containing 250 IU/mL RV IgG, which was beyond the linear range of the calibration curve (Fig. 2B). It is straightforward to dilute such samples on-chip—for example, to form 4 droplets of 125, 62.5, 15.6, and 31.3 IU/mL (see online Supplemental Fig. 2). Subsequently, RV IgG immunoassays can be performed on the diluted samples in parallel.

The assays described here were designed for application to patient serum and plasma samples. But for portable analysis in the field, it would be useful if the assay could also be used with whole blood, negating the requirement of phlebotomy (with finger stick) and fractionation. To evaluate this possibility, simulated whole blood samples (calibrator mixed with sheep's blood) were diluted on-chip and tested with the methods described above. As shown in Fig. 2C, the interassay CVs for these assays were only marginally higher in the blood samples (10% to 15%) than in the control (standard) samples (6% to 9%). Because of dissimilarities in matrix composition, the signal intensities of the calibrator samples differed significantly from the diluted samples containing high blood content (i.e., $P = 0.049$ for the 1/8 dilution and $P = 0.050$ for the 1/4 dilution). But when these samples were diluted further (i.e., 1/16 and 1/32 dilutions of blood), the results for blood and calibrator samples could not be distinguished ($P > 0.05$). These observations suggest that sample dilution may be useful for alleviating interferences arising from the blood matrix for application in the field, provided that the dilution does not reduce the analyte concentration below the LOQ of the assay.

RV IgM IMMUNOASSAY AND IgG BLOCKING

Whereas testing for RV IgG (described above) is useful for determining susceptibility and immune status, the critical test for diagnosing rubella-infected patients (including the identification of pregnancies at risk for CRS) is the detection of RV IgM. Unlike RV IgG, there is no agreed cutoff concentration for RV IgM to distinguish between negative or positive test results. As such, assay vendors develop their own cutoff calibrators on the basis of serological testing of samples obtained from healthy

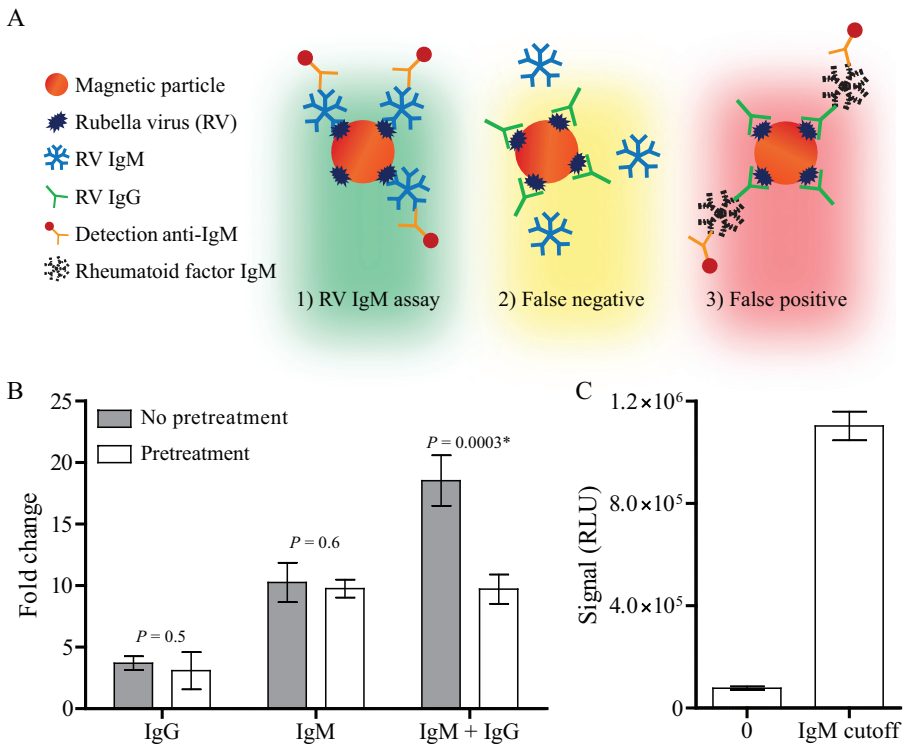

Fig. 3. RV IgM immunoassay.

(A), Scheme of RV IgM immunoassay (panel 1) and potential interferences or nonspecific interactions arising from the presence of RV IgG (panel 2) and RF IgM (panel 3). (B), Bar graph illustrating the effect of on-chip sample pretreatment (gray bars) relative to no pretreatment (white bars) in RV IgM immunoassays. (C), Diagnostic cutoff calibrator signal for RV IgM immunoassays implemented in digital microfluidics with sample pretreatment. Each value represents the mean (SD) from 3–4 replicates. Statistical significance (*$P < 0.05$) was evaluated by Student 2-tailed *t*-test.

and infected donors. In the assays reported here, the RV IgM Cal 1 reagent was adapted from the Abbott Architect rubella IgM assay kit to define the cutoff between positive and negative/equivocal results with digital microfluidics.

Similar to the RV IgG immunoassays described above, the on-chip RV IgM assays relied on RV-immobilized paramagnetic particles to implement indirect ELISA. In an ideal assay, RV IgM antibodies from the sample will bind to the particles, and the detection antibodies (HRP-conjugated antihuman IgM) will bind to the RV IgM to form immunocomplexes (Fig. 3A, panel 1). However, there are at least 2 potential sources of error in this assay scheme caused by the presence of RV IgG and/or RF IgM in human serum *(42)*. If the sample contains RV IgG, these antibodies will compete for binding sites on the particles, leading to false-negative results (Fig. 3A, panel 2). If the sample contains both RV IgG and RF IgM, immunocomplexes will form on the particles, leading to false-positive results (Fig. 3A, panel 3). Complicating matters, vendor-specific calibrators, which are formed from pooled human sera, often contain varying amounts of RF IgM or other cross-reactive species, depending on the source. To ascertain the presence of RF IgM in the calibrators used here, they were tested with an off-chip ELISA kit (see online Supplemental Table 1)—the RV IgG calibrators have low concentrations of RF IgM (1.4–1.85 IU/mL), and the RV IgM cutoff calibrator has high concentrations of RF IgM (27.0 IU/mL).

Fortunately, errors related to the presence of endogenous RV IgG and RF IgM (Fig. 3A) can be alleviated by pretreating the sample with exposure to exogenous antihuman IgG before analysis, which serves to block unwanted binding of RV IgG (and RV IgG/RF IgM complexes) onto the virus-laden particles *(4–6)*. Emulating the Architect rubella IgM assay procedures, we developed an on-chip pretreatment method in which a droplet of sample (1.8 μL) is mixed with a droplet of pretreatment reagent (900 nL, containing goat antihuman IgG) for 7 min before analysis by on-chip ELISA. To evaluate this

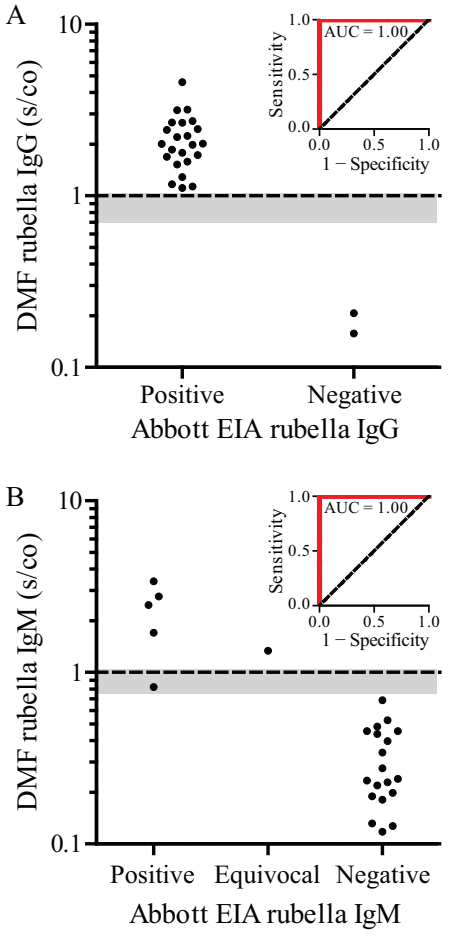

C

Sample	Rubella virus IgG		Rubella virus IgM	
	DMF s/co (result)	Abbott EIA s/co (result)	DMF s/co (result)	Abbott EIA s/co (result)
PTR201-01	1.3 (pos)	1.1 (pos)	0.2 (neg)	0.2 (neg)
PTR201-02	2.0 (pos)	2.4 (pos)	0.7 (neg)	0.5 (neg)
PTR201-03	4.6 (pos)	3.1 (pos)	2.8 (pos)	>2.3 (pos)
PTR201-04	2.2 (pos)	2.8 (pos)	0.1 (neg)	0.2 (neg)
PTR201-05	0.2 (neg)	0.1 (neg)	0.2 (neg)	0.1 (neg)
PTR201-06	1.2 (pos)	1.2 (pos)	0.2 (neg)	0.1 (neg)
PTR201-07	2.7 (pos)	2.5 (pos)	2.5 (pos)	1.2 (pos)
PTR201-08	2.0 (pos)	1.7 (pos)	0.1 (neg)	0.2 (neg)
PTR201-09	2.4 (pos)	2.7 (pos)	0.2 (neg)	0.1 (neg)
PTR201-10	1.7 (pos)	3.0 (pos)	0.1 (neg)	0.1 (neg)
PTR201-11	1.7 (pos)	2.7 (pos)	3.4 (pos)	>2.3 (pos)
PTR201-12	3.1 (pos)	2.7 (pos)	0.5 (neg)	0.2 (neg)
PTR201-13	2.4 (pos)	3.2 (pos)	0.2 (neg)	0.7 (neg)
PTR201-14	1.1 (pos)	2.4 (pos)	0.5 (neg)	0.1 (neg)
PTR201-15	2.7 (pos)	3.3 (pos)	0.4 (neg)	0.1 (neg)
PTR201-16	0.2 (neg)	0.1 (neg)	0.4 (neg)	0.2 (neg)
PTR201-17	2.0 (pos)	2.0 (pos)	0.5 (neg)	0.2 (neg)
PTR201-18	1.9 (pos)	1.1 (pos)	1.3 (pos)	0.9 (equ)
PTR201-19	2.2 (pos)	1.7 (pos)	1.7 (pos)	2.1 (pos)
PTR201-20	3.2 (pos)	>3.4 (pos)	0.2 (neg)	0.1 (neg)
PTR201-21	2.7 (pos)	2.2 (pos)	0.3 (neg)	0.2 (neg)
PTR201-22	1.1 (pos)	1.4 (pos)	0.5 (neg)	0.1 (neg)
PTR201-23	1.6 (pos)	2.2 (pos)	0.3 (neg)	0.1 (neg)
PTR201-24	1.5 (pos)	1.3 (pos)	0.8 (equ)	1 (pos)
PTR201-25	1.8 (pos)	2.5 (pos)	0.2 (neg)	0.3 (neg)

Result differs from Abbott EIA (determined by supplier)

Fig. 4. Performance of RV IgG and RV IgM immunoassay on commercial plasma/serum panel.

Plots of s/co values for DMF RV IgG (A) and RV IgM (B) immunoassays from RV mixed-titer panel (Seracare PTR201). Each DMF s/co value represents the mean from 3–4 replicates and is categorized as positive (pos), equivocal (equ), or negative (neg) on the basis of results from a leading commercial RV antibody immunoassay (Abbott EIA) determined by the supplier. DMF s/co values in the shaded region were interpreted as equivocal. The inset plots show the ROC curves for DMF assays (red lines) and random guesses (dashed lines). The area under the ROC curve (AUC) is reported in each plot. (C), Table comparing the results of the DMF and Abbott EIA assays. The s/co and interpretation of the Abbott EIA assays were supplied by Seracare. Shaded box indicates discrepancy in DMF assay with Abbott EIA.

method, we used test samples (formed from calibrators) containing RV IgG, RV IgM, or both RV IgG and RV IgM. As expected, the IgG-alone and IgM-alone sample results were unaffected by the pretreatment (Fig. 3B) because these samples did not contain high concentrations of RF IgM and RV IgG (see online Supplemental Table 1). In contrast, the pretreatment significantly ($P = 0.0003$) suppressed the nonspecific signal arising in the combined IgG plus IgM sample, which, as shown in online Supplemental Table 1, contains substantial concentrations of RV IgG (250 IU/mL) and RF IgM (approximately 14 IU/mL). Thus, accurate diagnosis of rubella infection requires IgG blocking, which is straightforward to implement and to establish cutoff values (Fig. 3C) in digital microfluidics.

EVALUATION OF DIAGNOSTIC ACCURACY

The diagnostic accuracies of the digital microfluidic RV IgG and IgM immunoassays were estimated with 25 plasma/serum samples from a commercial rubella mixed-titer performance panel (Fig. 4). These are undiluted aliquots of plasma or serum collected from individual donors between 1994 and 1995 by the vendor, used by diagnostic laboratories and manufacturers to evaluate their rubella tests. For each sample, the vendor provided reference results (s/co values and test interpreta-

tion) from tests performed by the vendor and independent reference laboratories (between 1995 and 1996) with several leading ELISA platforms at that time. In this study, the Abbott EIA test was chosen as the reference standard because test results were provided for both RV IgM and IgG.

In estimating diagnostic performance, all 25 samples were divided and tested for both RV IgG and RV IgM in 3–4 replicates to ascertain assay reproducibility. Typically, 4 parallel immunoassays, requiring approximately 25 (for RV IgG assays) or 35 (for RV IgM assays) min, were carried out in single (only RV IgG or RV IgM in quadruplicates) or duplex (both RV IgG and RV IgM in duplicates) format. The mean intraassay CV (range) was 4.6% (0.4%–17.5%) for RV IgG assays and 7.5% (1.5%–13.4%) for RV IgM assays. In the RV IgG assays (Fig. 4A), the DMF tests identified 23 positives, 0 equivocal, and 2 negatives, which represents perfect agreement with the Abbott EIA results. The diagnostic sensitivity and specificity (with 95% CIs) were 100% (98.6%–100%) and 100% (95.5%–100%), respectively (see online Supplemental Table 2). In the RV IgM assays (Fig. 4B), the DMF tests identified 5 positives, 1 equivocal, and 19 negatives, which represents close agreement with the Abbott EIA results (2 mismatches: 1 DMF equivocal/Abbott positive and 1 DMF positive/Abbott equivocal). In the calculation of diagnostic performance, the "equivocal" results (a classification not accounted for) were interpreted as "positive," yielding a sensitivity and specificity (with 95% CIs) of 100% (97.4%–100%) and 100% (98.4%–100%), respectively (see online Supplemental Table 3).

The measured s/co for all 25 samples tested are shown in Fig. 4C. For the 2 mismatches in the RV IgM assay, the DMF values (s/co = 0.9 and 1) were at or near the cutoff value (s/co = 1). Thus, we hypothesize that the discrepancy between the DMF and the standard results may be caused by a combination of assay variability (CV <15%) and degradation of the 20-year-old samples. Regardless, these types of positive-equivocal discrepancies represent a relatively minor problem, as in standard practice, all patients who test either positive or equivocal are retested to ascertain final diagnosis *(43)*.

The performance of the new DMF test (Fig. 4) was similar to that of central laboratory–based RV testing *(44)*. This is not surprising, since DMF, like automated immunoassay platforms, is automated and software programmable, allowing for integration of operations such as aliquoting, dilution, or IgG blocking as needed in an immunoassay work flow. More importantly, when compared with the only "rapid" rubella IgM test that we are aware of (Alere ImmunoComb® Rubella IgM), for which the manufacturer reports diagnostic sensitivity and specificity [sensitivity/specificity 87%/99% *(7)*], the DMF method has the added value of built-in, automated replicates and digital readout (i.e., no user interpretation of results). Of course, to further validate the diagnostic performance of the new method, additional testing must be performed in countries such as Vietnam, where rubella has not been introduced into the national immunization program *(45)*. Nevertheless, these initial results suggest that a portable DMF-based system, perhaps combined with inexpensive, paper devices *(29)*, may represent a useful new tool for identification of patients at risk for CRS in low-resource settings. More generally, we propose that similar methods might be useful for distributed diagnostics for a wide range of infectious diseases.

Author Contributions: *All authors confirmed they have contributed to the intellectual content of this paper and have met the following 3 requirements: (a) significant contributions to the conception and design, acquisition of data, or analysis and interpretation of data; (b) drafting or revising the article for intellectual content; and (c) final approval of the published article.*

Authors' Disclosures or Potential Conflicts of Interest: *Upon manuscript submission, all authors completed the author disclosure form. Disclosures and/or potential conflicts of interest:*

Employment or Leadership: None declared.
Consultant or Advisory Role: None declared.
Stock Ownership: A. Fischer, Abbott.
Honoraria: None declared.
Research Funding: This study was supported by the Natural Sciences and Engineering Research Council of Canada (NSERC) and Abbott Diagnostics. A. Ng, graduate fellowship from NSERC; A.R. Wheeler, Canada Research Chair Program.
Expert Testimony: None declared.
Patents: None declared.

Role of Sponsor: The funding organizations played no role in the design of study, choice of enrolled patients, review and interpretation of data, or preparation or approval of manuscript.

References

1. Gahr P, DeVries AS, Wallace G, Miller C, Kenyon C, Sweet K, et al. An outbreak of measles in an undervaccinated community. Pediatrics 2014;134:e220–e8.
2. WHO. WHO-recommended standards for surveillance of selected vaccine-preventable diseases. Geneva, Switzerland: World Health Organization, 2003.
3. WHO. Rubella. http://www.who.int/mediacentre/factsheets/fs367/en/ (Accessed September 2013).
4. McKenzie KG, Lafleur LK, Lutz BR, Yager P. Rapid protein depletion from complex samples using a bead-based microfluidic device for the point of care. Lab Chip 2009;9:3543–8.
5. Champsaur H, Fattal-German M, Arranhado R. Sensitivity and specificity of viral immunoglobulin M determination by indirect enzyme-linked immunosorbent assay. J Clin Microbiol 1988;26:328–32.
6. Meurman OH, Ziola BR. IgM-class rheumatoid factor interference in the solid-phase radioimmunoassay of rubella-specific IgM antibodies. J Clin Pathol 1978;31:483–7.
7. Alere(TM). ImmunoComb® rubella IgM. http://www.alere.com/ww/en/product-details/immunocomb-rubella-igm.html (Accessed July 2014).
8. Kiyaga C, Sendagire H, Joseph E, McConnell I, Grosz J,

Narayan V, et al. Uganda's new national laboratory sample transport system: a successful model for improving access to diagnostic services for early infant HIV diagnosis and other programs. PLoS One 2013;8:e78609.
9. Reef SE, Strebel P, Dabbagh A, Gacic-Dobo M, Cochi S. Progress toward control of rubella and prevention of congenital rubella syndrome: worldwide, 2009. J Infect Dis 2011;204:S24–S7.
10. Ng AHC, Uddayasankar U, Wheeler AR. Immunoassays in microfluidic systems. Anal Bioanal Chem 2010;397: 991–1007.
11. Shriver-Lake L, Golden J, Bracaglia L, Ligler F. Simultaneous assay for ten bacteria and toxins in spiked clinical samples using a microflow cytometer. Anal Bioanal Chem 2013;405:5611–4.
12. Phurimsak C, Yildirim E, Tarn MD, Trietsch SJ, Hankemeier T, Pamme N, Vulto P. Phaseguide assisted liquid lamination for magnetic particle-based assays. Lab Chip 2014;14:2334–43.
13. Martinez AW, Phillips ST, Butte MJ, Whitesides GM. Patterned paper as a platform for inexpensive, low-volume, portable bioassays. Angew Chem Int Ed 2007; 46:1318–20.
14. Pollock NR, Rolland JP, Kumar S, Beattie PD, Jain S, Noubary F, et al. A paper-based multiplexed transaminase test for low-cost, point-of-care liver function testing. Sci Transl Med 2012;4:152ra29.
15. Fu E, Liang T, Spicar-Mihalic P, Houghtaling J, Ramachandran S, Yager P. Two-dimensional paper network format that enables simple multistep assays for use in low-resource settings in the context of malaria antigen detection. Anal Chem 2012;84:4574–9.
16. Tekin HC, Gijs MAM. Ultrasensitive protein detection: a case for microfluidic magnetic bead-based assays. Lab Chip 2013;13:4711–39.
17. Chin CD, Cheung YK, Laksanasopin T, Modena MM, Chin SY, Sridhara AA, et al. Mobile device for disease diagnosis and data tracking in resource-limited settings. Clin Chem 2013;59:629–40.
18. Chin CD, Laksanasopin T, Cheung YK, Steinmiller D, Linder V, Parsa H, et al. Microfluidics-based diagnostics of infectious diseases in the developing world. Nat Med 2011;17:1015–9.
19. Jokerst JV, McDevitt JT. Programmable nano-biochips: multifunctional clinical tools for use at the point-of-care. Nanomedicine 2009;5:143–55.
20. Lafleur L, Stevens D, McKenzie K, Ramachandran S, Spicar-Mihalic P, Singhal M, et al. Progress toward multiplexed sample-to-result detection in low resource settings using microfluidic immunoassay cards. Lab Chip 2012;12:1119–27.
21. Fridley GE, Holstein CA, Oza SB, Yager P. The evolution of nitrocellulose as a material for bioassays. MRS Bull 2013;38:326–30.
22. Apilux A, Ukita Y, Chikae M, Chailapakul O, Takamura Y. Development of automated paper-based devices for sequential multistep sandwich enzyme-linked immunosorbent assays using inkjet printing. Lab Chip 2013; 13:126–35.
23. Lutz B, Liang T, Fu E, Ramachandran S, Kauffman P, Yager P. Dissolvable fluidic time delays for programming multi-step assays in instrument-free paper diagnostics. Lab Chip 2013;13:2840–7.
24. Whitesides GM. Viewpoint on "Dissolvable fluidic time delays for programming multi-step assays in instrument-free paper diagnostics." Lab Chip 2013;13: 4004–5.
25. Choi K, Ng AHC, Fobel R, Wheeler AR. Digital microfluidics. Annu Rev Anal Chem 2012;5:413–40.
26. Sista RS, Eckhardt AE, Wang T, Graham C, Rouse JL, Norton SM, et al. Digital microfluidic platform for multiplexing enzyme assays: implications for lysosomal storage disease screening in newborns. Clin Chem 2011;57:1444–51.
27. Srinivasan V, Pamula VK, Fair RB. An integrated digital microfluidic lab-on-a-chip for clinical diagnostics on human physiological fluids. Lab Chip 2004;4:310–5.
28. Cho SK, Moon H, Kim C-J. Creating, transporting, cutting, and merging liquid droplets by electrowetting-based actuation for digital microfluidic circuits. J Microelectromech Syst 2003;12:70–80.
29. Fobel R, Kirby AE, Ng AHC, Farnood RR, Wheeler AR. Paper microfluidics goes digital. Adv Mater 2014;26: 2838–43.
30. Fobel R, Fobel C, Wheeler AR. DropBot: an open-source digital microfluidic control system with precise control of electrostatic driving force and instantaneous drop velocity measurement. Appl Phys Lett 2013;102: 193513.
31. Peng C, Zhang Z, Kim CJ, Ju YS. EWOD (electrowetting on dielectric) digital microfluidics powered by finger actuation. Lab Chip 2014;14:1117–22.
32. Choi K, Ng AHC, Fobel R, Chang-Yen DA, Yarnell LE, Pearson EL, et al. Automated digital microfluidic platform for magnetic-particle-based immunoassays with optimization by design of experiments. Anal Chem 2013;85:9638–46.
33. Ng AHC, Choi K, Luoma RP, Robinson JM, Wheeler AR. Digital microfluidic magnetic separation for particle-based Immunoassays. Anal Chem 2012;84:8805–12.
34. Vergauwe N, Vermeir S, Wacker JB, Ceyssens F, Cornaglia M, Puers R, et al. A highly efficient extraction protocol for magnetic particles on a digital microfluidic chip. Sens Actuator B-Chem 2014;196:282–91.
35. Emani S, Sista R, Loyola H, Trenor CCI, Pamula VK, Emani SM. Novel microfluidic platform for automated lab-on-chip testing of hypercoagulability panel. Blood Coagul Fibrinolysis 2012;23:760–8.
36. Banoo S, Bell D, Bossuyt P, Herring A, Mabey D, Poole F, et al. Evaluation of diagnostic tests for infectious diseases: general principles. Nat Rev Microbiol 2008; 8:S16–S28.
37. WHO. Operational characteristics of commercially available assays to determine antibodies to HIV-1 and or HIV-2 in human sera. Report 11. Geneva, 1999.
38. Au SH, Kumar P, Wheeler AR. A new angle on pluronic additives: advancing droplets and understanding in digital microfluidics. Langmuir 2011;27:8586–94.
39. Fu E, Yager P, Floriano PN, Christodoulides N, McDevitt JT. Perspective on diagnostics for global health. IEEE Pulse 2011;2:40–50.
40. Dryden MD, Rackus DD, Shamsi MH, Wheeler AR. Integrated digital microfluidic platform for voltammetric analysis. Anal Chem 2013;85:8809–16.
41. Shamsi MH, Choi K, Ng AHC, Wheeler AR. A digital microfluidic electrochemical immunoassay. Lab Chip 2014;14:547–54.
42. Wilson D. Rheumatoid factors in patients with rheumatoid arthritis. Can Fam Phys 2006;52:180–1.
43. Tipples GA. Rubella diagnostic issues in Canada. J Infect Dis 2011;204:S659–S63.
44. Dimech W, Panagiotopoulos L, Francis B, Laven N, Marler J, Dickeson D, et al. Evaluation of eight anti-rubella virus immunoglobulin G immunoassays that report results in international units per milliliter. J Clin Microbiol 2008;46:1955–60.
45. Pham VH, Nguyen TV, Nguyen TTT, Dang LD, Hoang NH, Nguyen TV, Abe K. Rubella epidemic in Vietnam: characteristic of rubella virus genes from pregnant women and their fetuses/newborns with congenital rubella syndrome. J Clin Virol 2013;57:152–6.